Transition Metal Chemistry
https://doi.org/10.1007/s11243-019-00322-6

Syntheses, X-ray structures, electrochemical properties and biological evaluation of mono- and dinuclear N_2O_2-donor ligand-Fe systems

M. Venkata Nikhil Raj[1] · Kishalay Bhar[1] · Surbhi Jain[1] · Monika Rana[1] · Tanveer A. Khan[1] · Anuj K. Sharma[1]

Received: 18 January 2019 / Accepted: 4 April 2019

Abstract

The present work reports the synthesis, spectroscopic and structural characterizations of Fe(III) complexes of types [Fe(L)(H_2O)(NCS)] (**1**), [Fe(L)(1-methylimidazole)$_2$]ClO_4 (**2**) and [(L)Fe(μ-O)Fe(L)]·3H_2O·MeOH (**3**) containing a known planar N_2O_2-donor salphen Schiff base, H_2L (*N*,*N*′-bis(3-methoxysalicylidene)phenylene-1,2-diamine). In mononuclear complexes **1** and **2**, iron(III) centre adopts a distorted octahedral geometry where planar N_2O_2-donor L^{2-} ligand forms equatorial plane and varied co-ligands (aqua and thiocyanate in **1** and 1-methylimidazole in **2**) occupy the axial sites. The μ-oxo-bridged dinuclear complex **3** is a new solvatomorph of [(μ-O)(Fe(vanophen))$_2$]·2H_2O [vanophen = *N*,*N*′-bis(3-methoxysalicylidene)phenylene-1,2-diamine] reported by Jana et al. where a marked difference in Fe–O–Fe bond angle is noticed. The electrochemical behaviours of H_2L and complexes **1–3** have been examined to ascertain the nature of electron transfer processes. The binding interactions of **1–3** with ct-DNA as well as with Bovine serum albumin (BSA) have been investigated using fluorescence spectroscopy in $T_{10}E_1$ buffer (pH = 7.8). All the complexes show good binding propensity with ct-DNA probably via partial intercalation mode. Furthermore, the complexes quench the intrinsic fluorescence of BSA by a static quenching mechanism.

Introduction

Design and synthesis of iron(III) complexes with varied nuclearities is of continuous attention owing to their potential applications in catalysis [1, 2], enzyme mimicking [3, 4], molecular magnetism [5, 6] and drug designing [7–9]. Planar salen/salphen-type Schiff bases [10] are well suited for preparation of iron(III) complexes with diverse co-ligands like halide/pseudohalide and azole-based heterocycles. These metal–salen complexes containing planar aromatic rings have excellent binding ability with DNA typically through non-covalent (intercalation, electrostatic or groove binding) interactions [11–14]. Further, such redox-active transition metal complexes facilitate the generation of reactive oxygen species (ROS) under reducing environment causing the damage of DNA [12]. The potential anticancer activities of such iron(III)-salen/salphen complexes towards various human cancer cell lines (HOS, MCF-7, A549, HeLa, A2780 and G-361) have been well documented [7]. Importantly, the majority of complexes are highly cytotoxic and several fold more active than cisplatin [7], the well-known anticancer drug that has clinical use. In general, anticancer activity in such complexes depends upon the structure of the salen, nature and position of substituent on salen and co-ligands attached to the metal centre [15]. The presence of aromatic bridge between two imine N atoms in salen increases the anticancer activity [15], i.e. salphen is more effective than salen. Moreover, the redox properties associated with both metal and ligands in such complexes [9] may provide unusual mechanistic pathway for selective apoptosis and cytotoxicity towards cisplatin-resistant cancer cells. Of late, Lange et al. have reported an iron(III)–salphen complex, [Fe(L)(H_2O)(Cl)] (H_2L = *N*,*N*′-bis(3-methoxysalicylidene) phenylene-1,2-diamine) which shows selective cytotoxic effects [16] on human platinum-resistant ovarian cancer cells (SKOV-3 and OVCAR-3). Keeping in mind, all the above mentioned factors, particularly the drug designing and structural aspect of iron(III) salen/salphen complexes, here we have studied the coordination behaviour of H_2L ligand [16] towards iron(III) in combination with

Electronic supplementary material The online version of this article (https://doi.org/10.1007/s11243-019-00322-6) contains supplementary material, which is available to authorized users.

✉ Anuj K. Sharma
anuj.sharma@curaj.ac.in

[1] Department of Chemistry, School of Chemical Sciences and Pharmacy, Central University of Rajasthan, NH-8, Bandarsindri, Ajmer District, Rajasthan 305817, India

Published online: 15 April 2019

thiocyanate and 1-methylimidazole as co-ligands. Successfully, we have isolated two mononuclear compounds [Fe(L)(H_2O)(NCS)] (**1**) and [Fe(L)(1-methylimidazole)$_2$]ClO_4 (**2**), and a μ-oxo-bridged diiron(III) complex of the type [(L)Fe(μ-O)Fe(L)]·3H_2O·MeOH (**3**). The complexes are characterized through various physico-chemical and spectroscopic methods. The redox properties, ct-DNA and BSA binding studies of complexes **1–3** are delineated herein.

Experimental

Materials and methods

High-purity $(NH_4)_2SO_4.FeSO_4.6H_2O$ (Merck, India), $Fe(ClO_4)_2.6H_2O$ (Alfa Aesar, India), ortho-phenylenediamine (SRL, India), ortho-vanillin (Merck, India), 1-methylimidazole (Spectrochem, India) and potassium thiocyanate (Merck, India) were used as received. The Schiff base, *N*,*N*′-bis(3-methoxysalicylidene)phenylene-1,2-diamine (H_2L) was prepared using a reported method as described elsewhere [16, 17]. All other chemicals and solvents used were AR grade and used as received. The synthetic reaction and work-up were done in open air. Elemental analyses (CHNS) were performed on a Thermo-scientific flash 2000 elemental analyser. Infrared spectra were recorded at room temperature using PerkinElmer FTIR spectrometer (in KBr disc) in 4000–400 cm^{-1} range. The NMR spectra were recorded in $CDCl_3$ solvent on Bruker Avance III 500 MHz spectrometer at 25 °C. UV–Vis spectra and kinetic studies were performed at room temperature on Agilent Technologies Cary 100 UV–Vis spectrophotometer equipped with multiple cell holders. Fluorescence measurements were done on Agilent Technologies Cary Eclipse fluorescence spectrophotometer at 25 °C. Thermogravimetric analysis (TGA) was performed on a Discovery Thermogravimetric analyser by TA instruments-waters lab. All electrochemical experiments were performed with Autolab PGSTAT 302N workstation (Eco-Chemie BV, Netherlands). The electrochemical studies of ligand and complexes were carried out in dry acetonitrile and/or dry methanol, respectively, under nitrogen atmosphere at room temperature, at scan rate of 0.1 V/s in a three-electrode assembly using non-aqueous Ag/Ag^+ as reference electrode, glassy carbon as a working electrode and platinum wire as a counter electrode, with tetrabutylammonium perchlorate (TBAP) as the supporting electrolyte in the potential range from − 1 to 2 V, and were uncorrected for junction contributions. The value for the F_c–F_c^+ couple under our conditions is 0.47 V in MeOH and 0.44 V in MeCN [18]. CV data analyses were done using Nova 1.10.1.9 module provided with Autolab.

Synthesis

Synthesis of *N*,*N*′-bis(3-methoxysalicylidene) phenylene-1,2-diamine) (H_2L)

Ortho-vanillin (1.52 g, 10 mmol) dissolved in MeOH (10 ml) was added slowly to the solution of ortho-phenylenediamine (0.54 g, 5 mmol) in MeOH (10 ml) and stirred for 3 h at room temperature. Then, the orange crystalline solid was filtered off, washed with cold methanol and dried in vacuum. Yield: 1.31 g (70%). ^{1}H-NMR ($CDCl_3$): 13.22 (s, 2H, –OH), 8.63 (s, 2H, –CH=N–), 7.34 (m, 2H, –Ph), 7.20 (m, 2H, –Ph), 7.02 (dd, 2H, –Ph), 6.98 (dd, 2H, –Ph), 6.87 (t, 2H, –Ph), 3.90 (s, 6H, $–OCH_3$). FTIR (KBr disc, cm^{-1}): ν(HO) 3440, ν(C=N + C=C) 1626, 1584. UV–Vis [DMSO, λ_{max}/nm (ε/dm^3 mol^{-1} cm^{-1})]: 282 (3.0×10^4), 334 (2.3×10^4).

Synthesis of [Fe(L)(H_2O)(NCS)] (1)

To a light yellow aqueous-methanolic solution (10 ml) of $(NH_4)_2SO_4.FeSO_4.6H_2O$ (0.39 g, 1 mmol), an orange solution (15 ml) of H_2L (0.37 g, 1 mmol) in dichloromethane was added slowly followed by a colourless methanolic solution (10 ml) of KSCN (0.09 g, 1 mmol). The resulting dark green solution was filtered and kept for slow evaporation. After two days, dark plate-like crystals of **1** were isolated. Yield: 0.30 g (60%). Analytical calcd. for $C_{23}H_{20}N_3O_5SFe$ (506.33): C, 54.5; H, 3.9; N, 8.3; S, 6.3%. Found: C, 53.9; H, 3.8; N, 8.4; S, 6.5%. FTIR (KBr disc, cm^{-1}): ν(HO) 3400, ν(NCS) 2060, ν(C=N + C=C) 1605, 1577. UV–Vis [DMSO, λ_{max}/nm (ε/dm^3 mol^{-1} cm^{-1})]: 312 (3.7×10^4), 343 (2.4×10^4), 397 (1.3×10^4), 604 (2.3×10^3).

Synthesis of [Fe(L)(1-methylimidazole)$_2$]ClO_4 (2)

To an orange solution (20 ml) of H_2L (0.20 g, 0.53 mmol) in dichloromethane, a solution of $Fe(ClO_4)_2$ (0.14 g, 0.53 mmol) in methanol (10 ml) was added slowly. The colour of the mixture turned dark green. Then, a methanolic solution (10 ml) of 1-methylimidazole (0.09 ml, 1.06 mmol) was added to that mixture with continuous stirring. A dark greenish-brown solid was precipitated out immediately. The solid was isolated by filtration. The filtrate was kept for slow evaporation. After two days, dark green crystals of complex **2** were obtained. Yield: 0.20 g (55%). Analytical calcd. for $C_{30}H_{30}N_6O_8ClFe$ (693.90): C, 51.9; H, 4.3; N, 12.1. Found: C, 51.6; H, 4.1; N, 11.8. FTIR (KBr disc, cm^{-1}): ν(ClO_4) 1090, 623, ν(C=N + C=C) 1605, 1577. UV–Vis [DMSO, λ_{max}/nm (ε/dm^3 mol^{-1} cm^{-1})]: 311 (3.5×10^4), 343 (2.3×10^4), 397 (1.2×10^4), 604 (1.9×10^3).

Synthesis of [(L)Fe(μ-O)Fe(L)]·3H_2O·CH_3OH (3)

Complex **3** was isolated as dark brown crystalline solid by dropwise addition of water in excess to a dark green methanolic solution (0.20 g, 0.29 mmol) of complex **2** with continuous stirring until precipitation was completed. Yield: 0.10 g (71%) Analytical calcd. for $C_{45}H_{46}N_4O_{13}Fe_2$ (962.56): C, 56.1; H, 4.8; N, 5.8. Found: C, 55.9; H, 4.4; N, 5.5. FTIR (KBr disc, cm^{-1}): ν(HO) 3419, ν(C=N + C=C) 1603, 1580, ν(Fe–O–Fe) 854. UV–Vis [DMSO, λ_{max}/nm (ε/dm^3 mol^{-1} cm^{-1})]: 309 (6.5×10^4), 346 (4.6×10^4), 408 (2.2×10^4), 632 (1.9×10^3).

X-ray structure refinement

Crystallographic data of compounds **1–3** were collected on a Bruker Kappa APEX-II CCD diffractometer at 293(2) K (for **1**), 296(2) K (for **2**) and 100(2) K (for **3**) using graphite monochromated Mo Kα radiation ($\lambda = 0.71073$ Å). For unit cell determination, the single crystal was exposed to X-rays for 10 s in three sets of frames. The detector frames were integrated using SAINT program, and the multi-scan absorption corrections were performed using SADABS program [19]. The structures were solved by SHELXT [20] and refined by full-matrix least-squares methods based on F^2 using SHELXL [21]. All non-hydrogen atoms were refined with anisotropic displacement parameters, whereas hydrogen atoms were placed in calculated positions when possible and given isotropic U values 1.2 times that of the atom to which they are bonded. Materials for publication were prepared using PLATON [22] and OLEX2 [23] programs. A summary of the crystallographic data and structure determination parameters is given in Table 1.

DNA binding fluorescence quenching assay

The steady-state fluorescence quenching experiments were performed with ct-DNA on Agilent Technologies Cary

Table 1 Crystallographic data and refinement parameters for **1–3**

Crystal parameters	**1**	**2**	**3**
Formula	$C_{23}H_{20}FeN_3O_5S$	$C_{30}H_{30}ClFeN_6O_8$	$C_{45}H_{46}Fe_2N_4O_{13}$
Formula weight	506.33	693.90	962.56
Crystal system	Triclinic	Triclinic	Monoclinic
Space group	$P\bar{1}$	$P\bar{1}$	$P2_1/c$
a/Å	8.8035(3)	10.3441(5)	13.5531(15)
b/Å	11.4953(3)	10.4721(5)	22.894(3)
c/Å	11.8428(3)	15.1434(7)	14.7625(15)
α°	106.500(2)	99.255(2)	90
β°	99.689(2)	107.122(2)	112.774(4)
γ°	105.302(2)	93.316(3)	90
V/Å^3	1069.36(6)	1537.64(13)	4223.5(8)
λ/Å	0.71073	0.71073	0.71073
ρ_{calcd}/gm cm^{-3}	1.572	1.499	1.504
Z	2	2	4
T/K	293(2)	296(2)	100(2)
μ (mm^{-1})	0.845	0.639	0.760
F(000)	522	718	1976
θ ranges (°)	2.684–25.993	2.073–25.000	2.413–24.999
h/k/l	−10,10/−14,14/−14,14	−12,12/−12,12/−17,17	−16,16/−27,27/−17,17
Reflections collected	17,375	34,277	89,784
Independent reflections	4191	5389	7405
Data/restraints/parameters	4191/0/314	5389/6/427	7405/4/615
Goodness-of-fit on F^2	1.013	1.056	1.095
Final R indices [$I > 2\sigma(I)$]	$R_1 = 0.0369$	$R_1 = 0.0422$	$R_1 = 0.0449$
	$wR_2 = 0.0823$	$wR_2 = 0.1177$	$wR_2 = 0.1171$
R indices (all data)	$R_1 = 0.0531$	$R_1 = 0.0455$	$R_1 = 0.0537$
	$wR_2 = 0.0904$	$wR_2 = 0.1219$	$wR_2 = 0.1252$
Largest peak and hole (eÅ^{-3})	0.344 and −0.335	0.736 and −0.460	1.004 and −0.609
CCDC No.	1550383	1862333	1560868

Eclipse fluorescence spectrophotometer at room temperature. The samples were excited at 480 nm, and the emission was recorded from 490 to 800 nm ($\lambda_{emission} = 600$ nm). The excitation and emission slit width were fixed at 15 nm and 15 nm, respectively. Concentrated stock solutions (5 mM) of complexes **1–3** were prepared in DMSO. The titrations were carried out by adding increasing amount of complex into the solution of ct-DNA saturated with EtBr. The concentration of ct-DNA was fixed at 3.7×10^{-5} M. The DNA-EtBr solution was prepared in 10 mM Tris-1 mM EDTA ($T_{10}E_1$) buffer. A large range of complex-to-DNA molar ratio range was covered by varying the concentration of the complexes. DNA concentration per nucleotide was determined by recording the absorption spectra using 1 cm path length cuvettes. DNA solutions in 10 mM Tris/1 mM EDTA buffer gave a single peak for UV absorbance at 260 nm. The DNA concentration was determined by taking the molar absorption coefficient (ε_{260}) of ct-DNA as 6600 M^{-1} cm^{-1}. The concentration was calculated using the Beer–Lambert's Law:

$$A = \varepsilon cl$$

where A is the absorbance of the solution, ε is the molar absorption coefficient, c is the concentration of the solution and l is the path length of the cuvette. The concentration of DNA thus determined was 3.75×10^{-5} M.

BSA binding fluorescence quenching assay

The steady-state fluorescence quenching experiments were carried out on Agilent Technologies Cary Eclipse fluorescence spectrophotometer at room temperature. The excitation and emission slit widths were fixed at 15 and 3 nm, respectively. The concentrated stock solutions of all the three complexes were prepared in DMSO. Concentration of BSA was fixed at 3 µM, while the complex concentration was gradually increased from zero to nearly 50 µM which covered a large protein-to-complex ratio. The tryptophan residue of BSA was excited at 280 nm, and emission spectra were recorded from 285 to 510 nm. The final amount of DMSO in the solution was so small to affect any changes in the protein structure or conformation. The binding constant of interaction of iron complexes with BSA was determined by monitoring the intrinsic fluorescence of BSA solution with increasing complex concentration.

Results and discussion

Synthesis and formulation

The hexa-coordinated mononuclear complex **1** was obtained as a dark green crystalline solid in DCM-MeOH-H_2O (2:2:1) solvent mixture containing a 1:1:1 molar ratio of $(NH_4)_2SO_4{\cdot}FeSO_4{\cdot}6H_2O$, H_2L and KSCN. Complex **2** was isolated as dark green crystalline solid by reaction of a 1:1:2 molar ratio of $Fe(ClO_4)_2{\cdot}6H_2O$, H_2L and 1-methylimidazole in DCM-MeOH. The dark brown crystalline compound **3** was synthesised by dropwise addition of measured excess water to a methanolic solution of complex **2** with continuous stirring (Scheme 1). All the compounds are air stable and completely/partially soluble in common organic solvents like methanol, acetonitrile, dimethylsulphoxide and dimethylformamide, but insoluble in water. Elemental analyses of compounds **1–3** show good correspondence with the formulations.

Spectroscopic and thermal studies

In FTIR spectrum, free Schiff base (H_2L) displays ν(OH) stretching at 3440 cm^{-1} along with characteristic ν(C=N + C=C) bands at 1626 and 1584 cm^{-1} [17]. Complex **1** exhibits characteristic ν(C=N + C=C) peaks at 1605 and 1577 cm^{-1} of the deprotonated Schiff base [17]. In addition, **1** shows peak at 3400 cm^{-1} corresponding to ν(HO) stretching of water ligand [16]. In **1**, the metal bound thiocyanate bands for ν(NCS) and ν(C–S) appearing at 2060 cm^{-1} and 730 cm^{-1}, respectively, are indicative of N-bonded coordination [17] of thiocyanate to metal. In complex **2**, the stretching bands related to perchlorate counter anion appear at 1090 and 623 cm^{-1} along with characteristic ν(C=N + C=C) peaks of L^{2-} at 1605 and 1577 cm^{-1} [17]. FTIR spectrum of **3** shows moderately strong band at 854 cm^{-1} corresponding to ν(Fe–O–Fe) stretching [17]. In addition, broad band at around 3419 cm^{-1} is found in **3** which may correspond to ν(OH) stretching of crystalline water and methanol molecules [17]. In all cases, the characteristic ν(C=N + C=C) stretching frequency of Schiff base is shifted towards a lower energy region indicating involvement of the imine N atom in metal coordination [17]. In order to confirm the presence of crystalline solvent molecules in **3,** the thermogravimetric analyses (TGA) were carried out under N_2 atmosphere in the temperature range 34–700 °C. The TGA plot (Fig. 1) clearly shows the mass loss of 9.10% within the temperature range 37–100 °C corresponding to the loss of one methanol and three water molecules (calcd. 8.94%). Moreover, complex **3** shows thermal stability up to 310 °C and then started to decompose gradually. The electronic spectra of ligand (H_2L) and complexes (**1–3**) were recorded in DMSO at room temperature (Figure S1, supporting information). The ligand (H_2L) shows two bands around 282 nm and 334 nm which are attributed to $\pi \rightarrow \pi^*$ transitions [1, 24]. Hexa-coordinated mononuclear complexes [Fe(L)(NCS)(H_2O)] (**1**) and [Fe(L)(1-methylimidazole)$_2$](ClO_4) (**2**) exhibit one broad band and three shoulder bands. The first two bands observed at ~ 310 nm and ~ 345 nm are assigned to ligand-centred $\pi \rightarrow \pi^*$ transitions [1, 24]. The two other low-energy

Scheme 1 Synthetic routes for preparation of complexes **1–3**

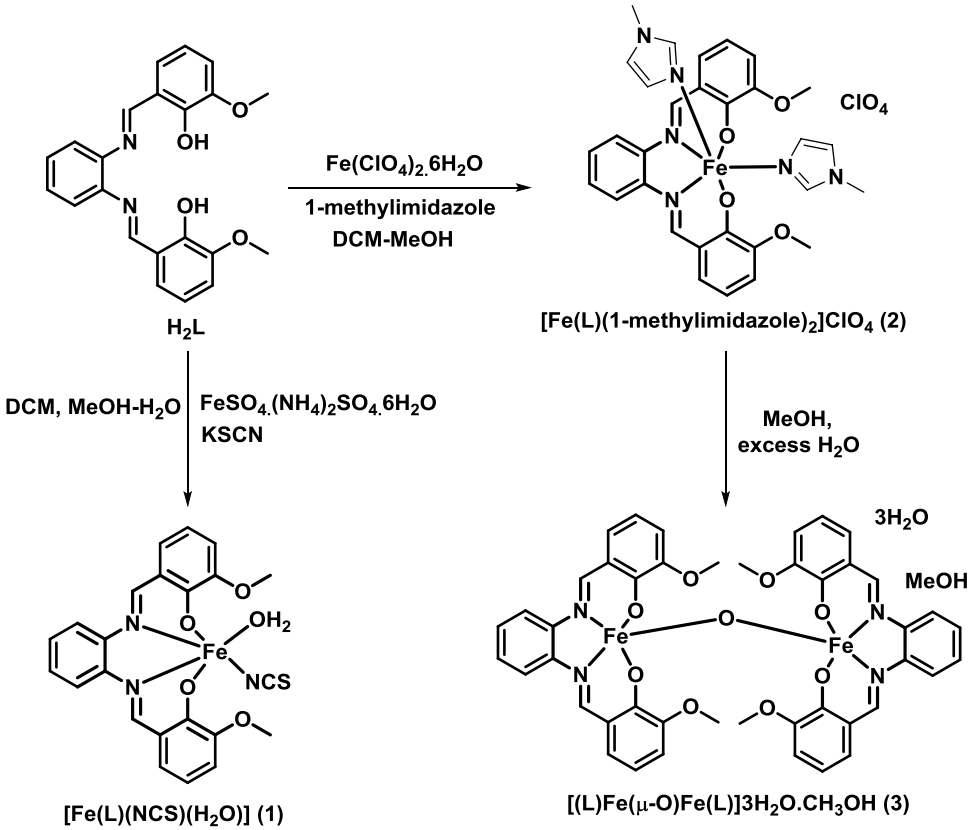

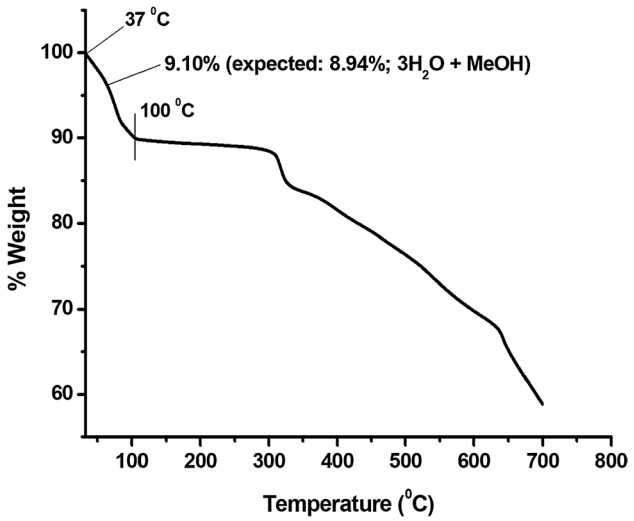

Fig. 1 TGA graph of compound **3** in the temperature range 34–700 °C

bands observed at ~400 nm and ~600 nm can probably be attributed to ligand-to-metal charge transfer (LMCT) transitions [1, 24–28] of the types $p\pi_{phenolate} \rightarrow d\sigma^*_{Fe}$ and $p\pi_{phenolate} \rightarrow d\pi^*_{Fe}$, respectively. The penta-coordinated dinuclear complex [(L)Fe(μ-O)Fe(L)]·3H_2O·MeOH (**3**) also shows one broad band and three shoulder bands. The first two bands observed at 309 nm and 346 nm can be assigned to ligand-based $\pi \rightarrow \pi^*$ transitions [1, 24]. The shoulder band appeared at 408 nm is probably attributed to $p\pi_{phenolate} \rightarrow d\sigma^*_{Fe}$ phenolate ligand-to-metal charge transfer (LMCT) transition [24–28]. The second shoulder band appeared at 632 nm can be attributed to $p\pi_{phenolate} \rightarrow d\pi^*_{Fe}$ LMCT and weaker oxo-to-iron CT transition [24–28].

Crystal structures of [Fe(L)(H_2O)(NCS)] (1) [Fe(L)(1-methylimidazole)$_2$]ClO_4 (2), [(L)Fe(μ-O)Fe(L)]3H_2O·CH_3OH (3)

Single crystal X-ray structures have been determined to unravel the coordination geometry and nuclearity of complexes **1–3**.

Complex **1** is the thiocyanate analogue of a chloro complex [Fe(L)(H_2O)(Cl)] reported [16] by Lange et al. Structural analysis of **1** reveals an asymmetric unit consisting of a [Fe(L)(H_2O)(NCS)] molecule. The coordination polyhedron around iron(III) is best described as a distorted octahedron with a FeN_3O_3 chromophore. The coordination sphere includes two imine N atoms (N2 and N3) and two O atoms (O1 and O2) of Schiff base ligand, one N atom (N3) of terminal NCS unit and one O atom (O5) of water (Fig. 2). Two imine N atoms (N2 and N3) along with two O atoms (O1 and O2) of the Schiff base define the equatorial plane, while one

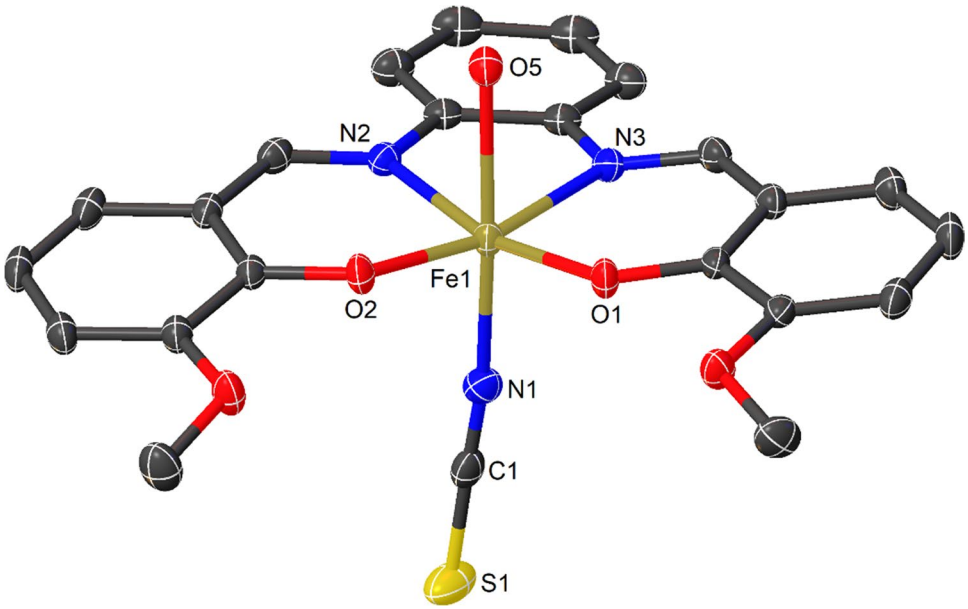

Fig. 2 Molecular structure of **1**

aqua molecule (O5) and one thiocyanate (N1) anion are in the axial positions. Fe(III) centre deviates (0.148 Å) slightly from the mean basal plane towards axial thiocyanate. The Fe–O and Fe–N bond distances (Table S1) are in line with the high-spin Fe(III) [17]. The structural features of complex **1** are comparable with the chloro analogue [16].

Complex **2** is the 1-methylimidazole analogue of a reported imidazole iron(III) complex [17] by Jana et al. Structural analysis shows that complex [Fe(L)(1-methylimidazole)$_2$]ClO_4 (**2**) crystallizes in a triclinic system with $P\bar{1}$ space group. The Fe(III) centre adopts a distorted octahedral geometry coordinated by N_2O_2-donor set (N3, N4, O1, O2) of the deprotonated Schiff base along the basal plane and two N atoms (N1, N2) of two 1-methylimidazole moieties in axial positions (Fig. 3). The Fe–O and Fe–N bond distances (Table S1) are in line with the high-spin Fe(III) [17]. The

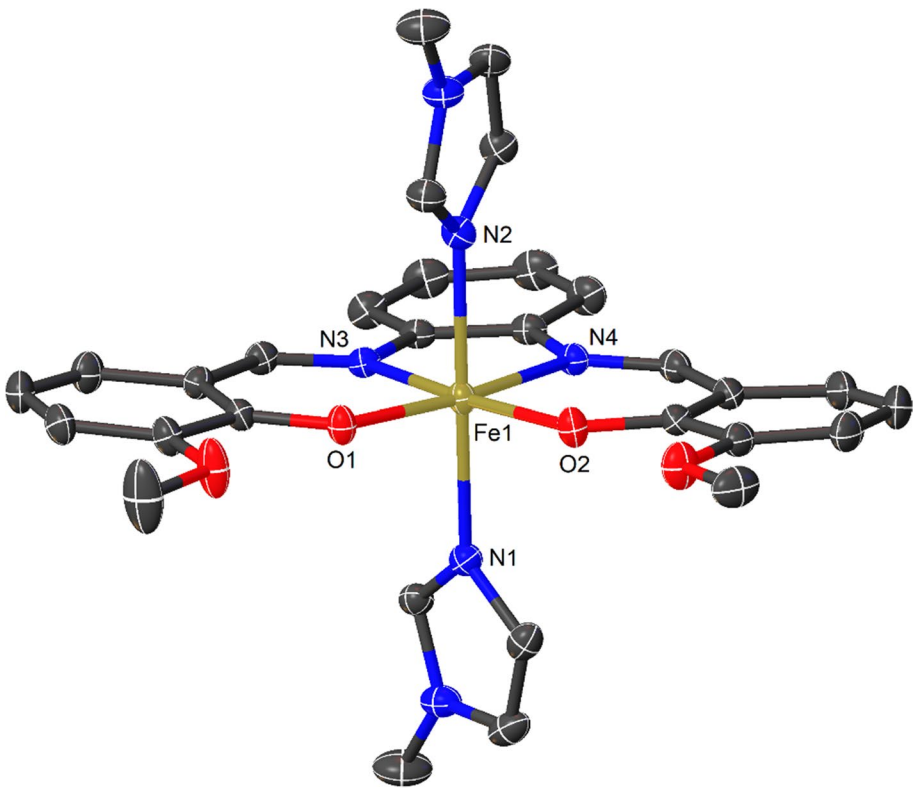

Fig. 3 Molecular structure of [Fe(L)(1-methylimidazole)$_2$]$^+$ in **2**

Fe1 centre deviates (0.009 Å) slightly from the mean basal plane. Two 1-methylimidazole rings are almost orthogonal (dihedral angle: 65.16°) to each other. The structural features of complex **2** are comparable with the imidazole analogue [17].

It is worth to mention that complex **3** isolated here is a solvatomorph [29] of the oxo-bridged compound reported [17] by Jana et al. Complex **3** is a μ-oxo-bridged dinuclear Fe(III) compound. The asymmetric unit of **3** consists of a [(L)Fe(μ-O)Fe(L)] dimeric unit with a crystalline methanol and three water molecules (Fig. 4). The iron(III) centres (Fe1 and Fe2) surrounded by the four coordinating atoms N_2O_2 of the ligand, extend towards the bridging oxygen atom as much as 0.565 Å and 0.560 Å, respectively. Two FeN_2O_2 cores are in staggered orientation relative to the oxo-bridge to minimize interligand steric repulsions. The overlay plot of two solvatomorphs is given in Fig. 5a demonstrating different orientations (Green: complex **3** and Pink: reported solvatomorph). It is found that two FeN_2O_2 cores in **3** are in staggered orientation which enables two vanillin units from each FeN_2O_2 core to involve in both intra- [Cg(9)–Cg(10): 3.600(2) Å, dihedral angle (α): 8.86(18)°, slippage: 1.056 Å, symmetry code: *x*, *y*, *z*; Cg(9): C15–C16–C17–C18–C19–C20; Cg(10): C21–C22–C23–C24–C25–C26] and intermolecular [Cg(9)–Cg(9): 3.676(2) Å, dihedral angle (α): 0°, slippage: 1.639 Å, symmetry code: −x, 1−y, 1−z] π–π stacking interaction (Fig. 5b). Such staggered orientation and intramolecular π–π stacking are primarily responsible in stabilizing the bent μ-oxo-bridge with a Fe–O–Fe angle 136.86(13)° in **3**. On the contrary, the orientation of FeN_2O_2 cores is in between eclipsed and staggered orientations in the reported solvatomorph [17] which prevents such intramolecular π–π stacking interaction. This results in a higher Fe–O–Fe bond angle [154.3(2)°] in the reported solvatomorph. In **3**, the structural distortion indexes are found as τFe1 = 0.19 and τFe2 = 0.02, respectively, which indicates that Fe1 and Fe2 polyhedra are all close to a distorted square pyramid. To the best of our knowledge, the Fe–O–Fe bond angle [136.86(13)°] and Fe···Fe distance (3.326 Å) in **3** are shortest compared to those of structurally related dinuclear complexes (Table S2) with the Fe–O–Fe bridge.

Redox behaviour of H_2L and complexes 1–3

Cyclic voltammograms were recorded for H_2L (in acetonitrile) and complexes [Fe(L)(NCS)(H_2O)] (**1**), [Fe(L)(1-methylimidazole)$_2$](ClO_4) (**2**) and [(L)Fe(μ-O)Fe(L)]·3H_2O·MeOH (**3**) (in methanol) to investigate ligand and/or metal-centred redox behaviours. Ligand, H_2L having two phenolate groups shows two irreversible oxidative responses (Figure S2a) at 0.99 V and 1.54 V versus Ag/Ag^+ in acetonitrile probably due to formation of phenoxy radicals. Similarly, complexes **1–3** show two irreversible oxidative responses (Figures S2b–S2d) in the potential range 1.10–1.40 V versus Ag/Ag^+ in methanol. Such values are in line with some reported complexes containing salen/salphen-type ligand systems [30]. Two mononuclear complexes **1** and **2** in methanol show one irreversible reductive response at −0.49 V and −0.55 V versus Ag/Ag^+,

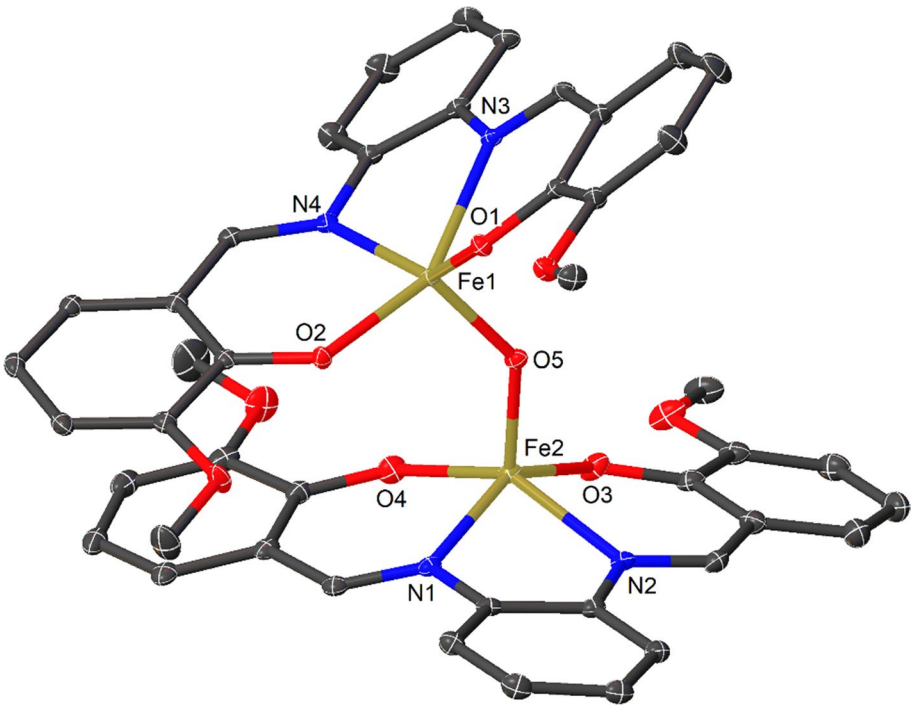

Fig. 4 A view of μ-oxo-bridged dinuclear structure in **3**

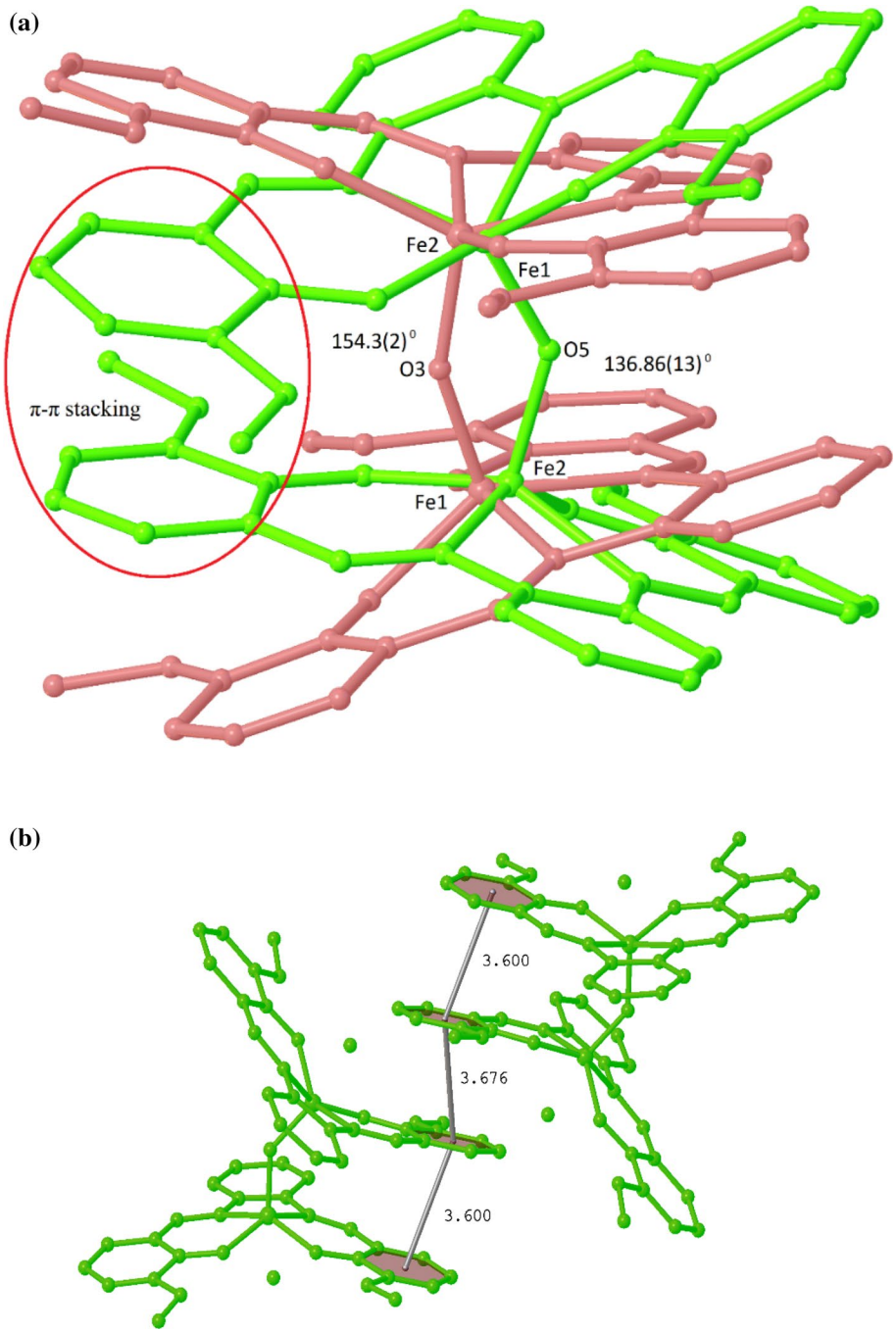

Fig. 5 **a** An overlay view of complex **3** (green) and reported complex of Jana et al. [17] (pink) (CIF BEHJIJ 870310 of the reported complex by Jana et al. [17] was obtained from CCDC and the structures were drawn using OLEX2 [23] program); **b** A view of intramolecular π–π stacking in **3** which is primarily responsible in stabilizing the bent μ-oxo-bridge

respectively (Figure S3), which may be originated from the metal-centred reduction of Fe(III) → Fe(II). A similar type of cathodic response was observed in reported [Fe(dmsalen)(H_2O)(Cl)] complex [26]. The dinuclear complex [(L)Fe(μ-O)Fe(L)]·3H_2O·MeOH (**3**) in methanol also shows one irreversible reductive response at − 0.47 V (Fig. 6) which is attributed to the metal-centred reduction of Fe(III) → Fe(II) [31].

DNA-binding interactions

Transition metal complexes can bind to DNA via both covalent (replacement of a labile coordinating ligand by nitrogen base of DNA) and/or non-covalent (intercalation, electrostatic or groove binding) interactions [32]. Many important applications emerge if the complexes can bind to DNA via

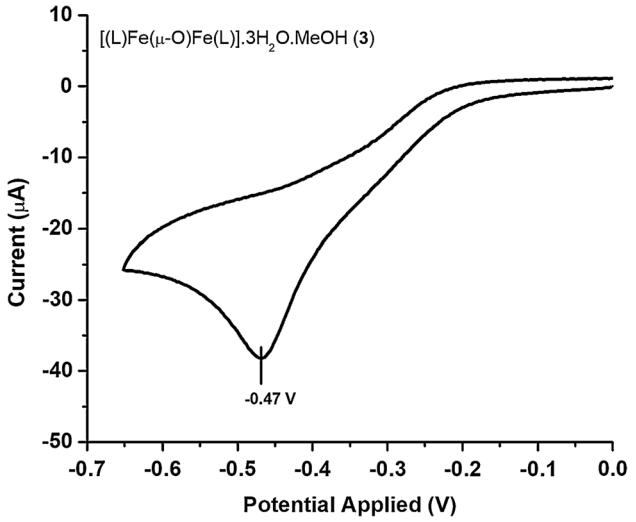

Fig. 6 Cyclic voltammogram of [(L)Fe(μ-O)Fe(L)]·$3H_2O$·MeOH (**3**) (0.5×10^{-3} M) at scan rate of 0.1 V/s recorded in methanol using Ag/Ag^+ as reference electrode, Glassy carbon as working electrode, Pt wire as a counter electrode and TBAP as supporting electrolyte

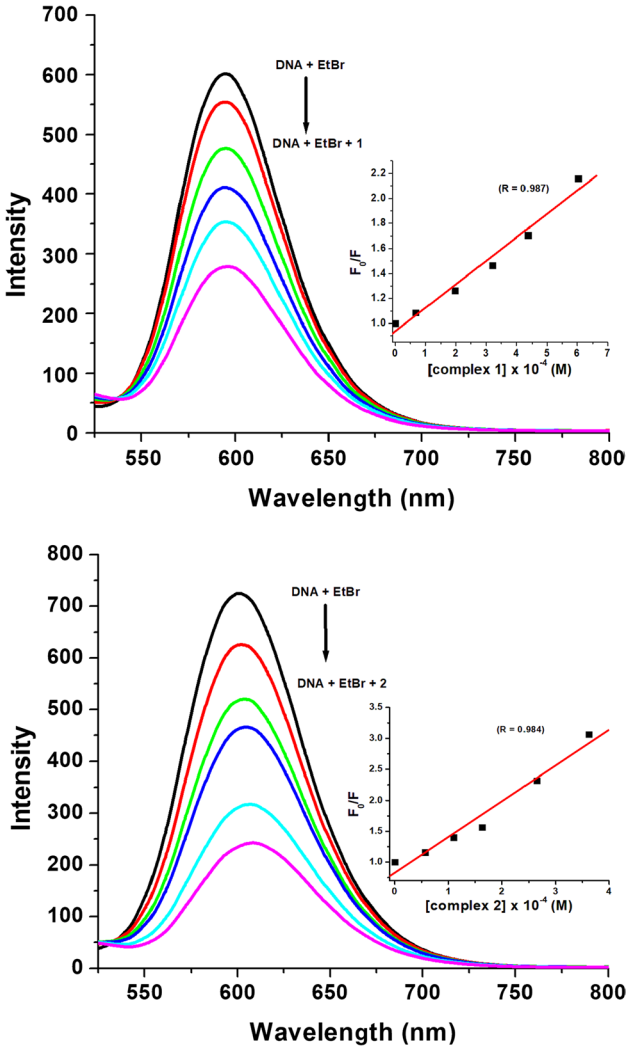

Fig. 7 Fluorescence intensity versus wavelength plot for DNA-EtBr solution at different concentrations of mononuclear complexes **1** (Top) and **2** (Bottom). The arrow shows change in intensity of DNA-EtBr emission upon increasing amount of compound. Inset: the plot of F_0/F versus the complex concentration

an intercalative mode [32]. Therefore, the interaction of metal complexes, especially when containing planar aromatic heterocyclic ligands which can insert and stack themselves into the base pairs of the DNA duplex has attracted considerable attention [32]. A competitive ethidium bromide (EtBr or 3,8-Diamino-5-ethyl-6-phenylphenanthridinium bromide) binding study has been carried out with fluorescence experiment in order to investigate if the complex could displace EtBr from its EtBr-DNA complex. EtBr is a typical indicator of intercalation [11–14]. The molecular fluorophore EtBr forms soluble complexes with nucleic acids and emits intense fluorescence in the presence of ct-DNA due to the intercalation of the planar phenanthridinium ring between adjacent base pairs on the double helix. In order to investigate the binding ability of iron complexes **1–3**, they were titrated with the solution of ct-DNA-EtBr (see experimental). The fluorescence of EtBr enhances upon intercalation with ct-DNA which can be hampered by another DNA-binding molecule which in our case are the synthesized iron(III) complexes. The competitive binding of the complexes **1–3** to ct-DNA quenched the emission intensity of EtBr. The fluorescence intensity of EtBr at 600 (480 nm excitation) with an increasing amount of the complex concentration was recorded. The fluorescence quenching curve of EtBr-bound ct-DNA in the presence of complexes **1–3** is in good agreement with the classical linear Stern–Volmer equation [11, 14]: $F_0/F = 1 + K_{SV}$[complex], where F_0 is the emission intensity of ct-DNA-EtBr in the absence of complex and F is the emission intensity of ct-DNA-EtBr in the presence of complex. The linear plot of F_0/F versus [complex] gives a measure of the fluorescence intensity changes (Figs. 7 and 8). The K_{SV} values of the complexes were calculated as 1.88×10^3 ($R = 0.987$ for initial six points) for **1**, 5.78×10^3 ($R = 0.984$ for initial six points) for **2** and 9.92×10^3 ($R = 0.990$ for initial six points) for **3**. By considering a DNA-binding constant of 1.0×10^7 M^{-1} for EtBr and the complex concentration of the value at a 50% reduction in the fluorescence intensity of EtBr, an apparent DNA-binding constant K_{app} of the complexes (1.77×10^5 M^{-1} for **1**, 4.41×10^6 M^{-1} for **2** and 5.96×10^6 M^{-1} for **3**) was derived from the equation: K_{EtBr}[EtBr] = K_{app}[complex], which is less than the binding constant of classical intercalations. This suggests that the complexes interact moderately with ct-DNA. The apparent DNA-binding constant K_{app} of some reported salen/salphen Schiff base complexes [11–13, 33, 34] falls in the range 1×10^4–1.6×10^6 M^{-1}. As compared

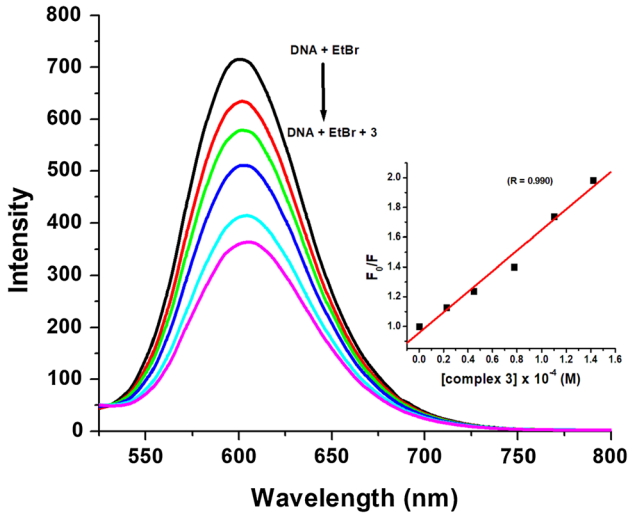

Fig. 8 Fluorescence intensity versus wavelength plot for DNA-EtBr solution at different concentrations of dinuclear complex **3**. The arrow shows change in intensity of DNA-EtBr emission upon increasing amount of compound. Inset: the plot of F_0/F versus the complex concentration

with the reported examples, the apparent binding constant (K_{app}) values of complexes **1–3** indicate that the complexes partially intercalate with the DNA helix [11, 14, 33]. Also, the relatively higher binding propensity of complexes **1–3** to ct-DNA can be ascribed due to the presence of planar aromatic moieties. Further, the values of binding constant (K_a) and number of binding sites (n) for ct-DNA–complex interactions were calculated from the fluorescence data using the Scatchard Eq. (1) [11].

$$\log\left(\frac{F_o - F}{F}\right) = \log K_a + n\log[Q] \quad (1)$$

where F_o and F are fluorescence intensities of ct-DNA-EtBr solution in the absence and presence of varying concentrations of complexes **1**, **2** or **3**. [Q] is the concentration of the quencher. The Scatchard plots for complexes **1–3** are given in supporting information (Figures S4 and S5). The values of K_a and n obtained from intercept and slope of Scatchard plot are summarized in Table 2. The binding constant values are in the range of 10^4–10^5 M^{-1} which shows the possibility of intercalative binding [11]. The value of n is in the range of 1.39–1.56, which suggests the presence of more than one binding site for interaction of **1–3** with ct-DNA. It also indicates the existence of moderate interactions between complexes **1–3** and ct-DNA. Further, binding affinity of **1–3** with DNA follows the order **3 > 2 > 1**. These results are in good agreement with the geometry and nuclearity of the complexes. The penta-coordinated dinuclear complex **3** has higher binding affinity as compared to mononuclear hexa-coordinated complexes **1** and **2**. Moreover, the binding affinity of **2** is higher than **1** which can probably be due to the presence of aromatic 1-methylimidazole moieties in axial positions.

BSA binding studies

Serum albumins are the carriers of essential metal ions in the body and are the most abundant proteins in blood and cerebrospinal fluid. Interactions between serum albumin and chemicals have attracted many researchers as serum albumin plays a crucial role in drug transport and drug metabolism [11, 14, 35]. Serum albumin is also well known to bind small molecules with aromatic moieties. Bovine serum albumins (BSA) is the most extensively studied serum albumin due to its structural homology with human serum albumin (HSA) [11, 14, 35]. Their binding with drugs is important as it can alter the efficiency of the drug. A strong fluorescence emission at 345 nm is observed in BSA solutions when excited at 280 nm due to the presence of tryptophan residues. The fluorescence intensity of BSA solution decreases gradually by adding an increasing amount of iron(III) complexes (**1–3**) (Figs. 9 and 10). The observed quenching may be attributed to substrate binding, subunit association, denaturation of protein or changes in the secondary protein conformation [11, 14, 35]. The fluorescence quenching is quantitatively calculated by the Stern–Volmer equation, $F_0/F = 1 + K_q\tau_0[Q] = 1 + K_{SV}[Q]$, where F_0 and F represent the fluorescence intensities in the absence and in the presence of quencher, K_q is the quenching rate constant, τ_0 the average lifetime of the biomolecule without quencher (about 10^{-8} s) [11], K_{SV} the Stern–Volmer quenching constant, and [Q] the concentration of quencher. The calculated values of K_{SV} and K_q are given in Table 2. The calculated K_q value for the BSA complex systems of **1–3** is in the magnitude of 10^{13} M^{-1} s^{-1}, which is threefold higher than 2.0×10^{10} M^{-1} s^{-1}, the maximum scatter collision quenching constant of quenchers with BSA. This result is indicative of the existence of static quenching.

Table 2 DNA and BSA binding parameters of complexes **1–3**

DNA					BSA			
Complex	K_{SV} (M^{-1})	K_{app} (M^{-1})	K_a (M^{-1})	N	K_{SV} (M^{-1})	K_q ($M^{-1}s^{-1}$)	K_a (M^{-1})	f_a
1	1.88×10^3	1.77×10^5	4.17×10^4	1.39	1.61×10^5	1.61×10^{13}	1.27×10^5	1.09
2	5.78×10^3	4.41×10^6	5.38×10^5	1.56	1.68×10^5	1.68×10^{13}	1.41×10^5	1.05
3	9.92×10^3	5.96×10^6	7.72×10^5	1.50	3.04×10^5	3.04×10^{13}	1.42×10^5	1.21

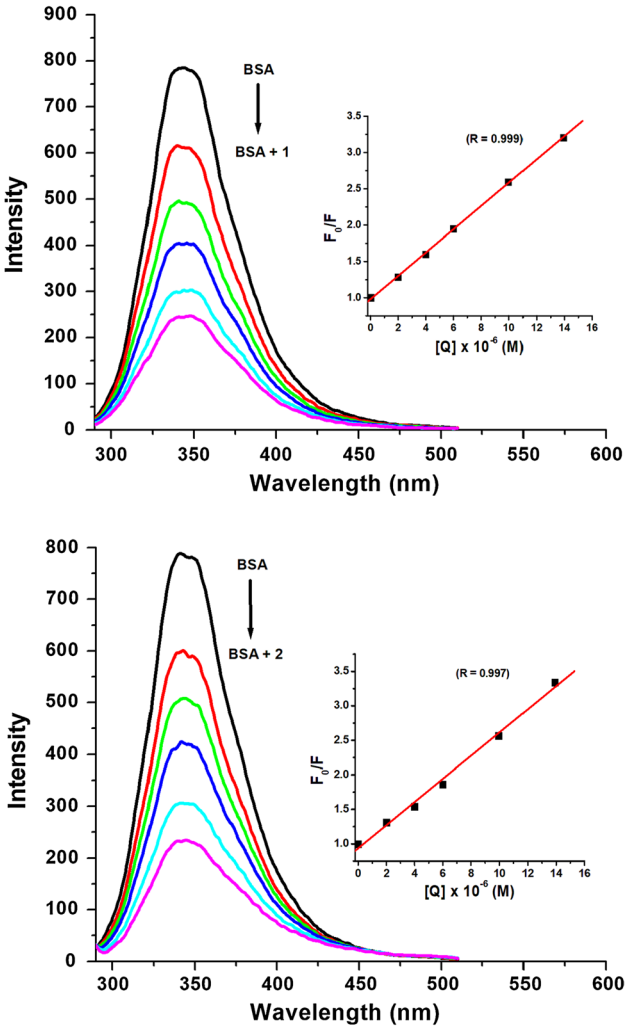

Fig. 9 Fluorescence intensity versus wavelength plot for BSA solution at different concentrations of complexes **1** (Top) and **2** (Bottom). The arrow shows change in intensity of BSA emission upon increasing amount of compound. Inset: the plot of F_0/F versus the complex concentration

Further, the binding constant (K_a) was calculated using modified Stern–Volmer (MSV) Eq. (2) [35].

$$\frac{F_0}{F_0 - F} = \frac{1}{K_a f_a [Q]} + \frac{1}{f_a} \quad (2)$$

where F_o is the initial tryptophan fluorescence intensity of BSA, F is the tryptophan fluorescence intensity of BSA after addition of complexes **1**, **2** or **3** acting as a quencher, f_a is the fraction of the tryptophan that is initially accessible to the complex and [Q] the concentration of the quencher. The linearity in the MSV plots of all three complexes is also indicative of possible static quenching mechanism [11]. The ratio of intercept to slope of MSV plots (Figures S6 and S7) gave the effective binding constant (K_a) values (Table 2) for

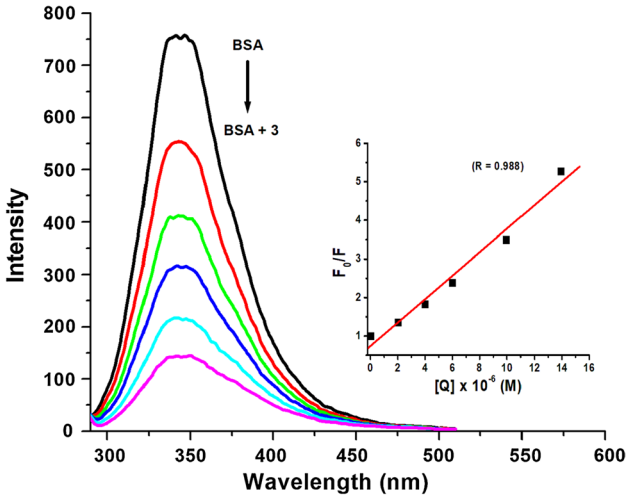

Fig. 10 Fluorescence intensity versus wavelength plot for BSA solution at different concentrations of complex **3**. The arrow shows change in intensity of BSA emission upon increasing amount of compound. Inset: the plot of F_0/F versus the complex concentration

complex BSA binding. Complexes show good binding affinity towards BSA with binding constant value in the order of 10^5 M^{-1}. The value of f_a is close to 1 indicating the presence of single binding site for interaction of **1–3** with BSA. In comparison with some reported iron(III)–salen complexes [11] (3.6×10^4–1.36×10^5 M^{-1}), the binding constant values for complexes **1–3** are similar.

Conclusion

In summary, we have synthesized and characterized two hexa-coordinated mononuclear complexes [Fe(L)(H_2O)(NCS)] (**1**) and [Fe(L)(1-methylimidazole)$_2$]ClO_4 (**2**), and one penta-coordinated dinuclear μ-oxo-bridged complex [Fe_2(L)$_2$(μ-O)]·3H_2O·CH_3OH (**3**) of iron(III) in combination with a salphen (N_2O_2-donor) Schiff base. The dinuclear complex **3** was isolated using a new synthetic strategy that resulted in a solvatomorph of the reported complex [(μ-O)(Fe(vanophen))$_2$]·2H_2O by Jana et al. Structural studies show a marked difference in Fe–O–Fe bond angle (136.86(13)°) in **3** compared to the reported solvatomorph (154.3(2)°). The intramolecular π–π stacking in staggered orientation between two vanillin rings of FeN_2O_2 cores plays a major role for such lowering in Fe–O–Fe bridging angle. The ct-DNA and BSA binding interactions of the mono- and dinuclear iron(III) (**1–3**) complexes were studied. The dinuclear iron(III) complex **3** showed significant ct-DNA and BSA binding propensity than the mononuclear iron(III) complexes **1** and **2**. The studies suggested that co-ligands, nuclearity and geometry of iron(III) complexes play noticeable role in the binding interactions with both ct-DNA and BSA.

Further, biological studies especially anticancer studies are in progress and will be reported elsewhere.

Supporting information

Crystallographic data for the structural analysis have been deposited with the Cambridge Crystallographic Data Centre CCDC Nos. 1550383 (1), 1862333 (2) and 1560868 (3). Copy of this information can be obtained free of charge from The Director, CCDC, 12 Union Road, Cambridge, CB2 1EZ, UK (fax: +44-1223-336033; e-mail: deposit@ccdc.cam.ac.uk or http://www.ccdc.cam.ac.uk). Additionally, the graph of UV–Visible spectra (ligand and complexes **1–3**), table of selected bond distances and angles for complexes **1–3**, table of some structurally related μ-oxo-bridged compounds and their Fe–O–Fe bridging features, CV spectra (ligand and complexes **1–3**), Scatchard plots for DNA-binding studies (complexes **1–3**) and modified Stern–Volmer (MSV) plots for BSA binding studies (complexes **1–3**) are submitted.

Acknowledgements AKS acknowledges Science and Engineering Research Board for financial support (grant ref.: EMR/2016/001452) and DST-INSPIRE research grant (IFA-13, CH-97). VNR is grateful to Central University of Rajasthan for University fellowship. SJ thanks DST-INSPIRE for SRF; MR is thankful to DST-SERB for fellowship; TAK is grateful to the UGC for SRF; KB is grateful to SERB for NPDF (PDF/2017/000929) fellowships. Authors acknowledge the instrumental facilities at Department of Chemistry, Central University of Rajasthan supported by DST-FIST (ref. no. SR/FST/CSI-257/2014 (C)). We are thankful to Department of Chemistry, IIT, Jodhpur and USIC, The University of Burdwan for X-ray crystallographic facilities. Paper is dedicated to the memories of Dr. Sunil G. Naik. The authors also acknowledge the Reviewers for their valuable suggestions in the revision stage.

Compliance with ethical standards

Conflicts of interest There are no conflicts of interest to declare.

References

1. Cozzolino M, Leo V, Tedesco C, Mazzeo M, Lamberti M (2018) Dalton Trans 47:13229–13238
2. Karimpour T, Safaei E, Karimi B, Lee YI (2018) ChemCatChem 10:1889–1899
3. Pathak C, Gupta SK, Gangwar MK, Prakasham AP, Ghosh P (2017) ACS Omega 2:4737–4750
4. Chatterjee S, Sukul D, Banerjee P, Adhikary J (2018) Inorg Chim Acta 474:105–112
5. Boonprab T, Harding P, Murray KS, Phonsri W, Telfer SG, Alkaş A, Ketkaew R, Tantirungrotechai Y, Jameson GN, Harding DJ (2018) Dalton Trans 47:12449–12458
6. Mondal D, Majee MC, Kundu S, Mörtel M, Abbas G, Endo A, Khusniyarov MM, Chaudhury M (2018) Inorg Chem 57:1004–1016
7. Wani WA, Baig U, Shreaz S, Shiekh RA, Iqbal PF, Jameel E, Ahmad A, Mohd-Setapar SH, Mushtaque M, Hun LT (2016) New J Chem 40:1063–1090
8. Chanu SB, Banerjee S, Roy M (2017) Eur J Med Chem 125:816–824
9. Zhang P, Sadler PJ (2017) Eur J Inorg Chem 2017:1541–1548
10. Cozzi PG (2004) Chem Soc Rev 33:410–421
11. Wang BW, Jiang L, Dong Z, Li BW, Shu SS, Gu W, Liu X, Tian JL (2014) J Coord Chem 67:2062–2075
12. Ali A, Kamra M, Bhan A, Mandal SS, Bhattacharya S (2016) Dalton Trans 45:9345–9353
13. Shahabadi N, Ghasemian Z, Hadidi S (2012) Bioinorg Chem Appl 2012:1–9
14. Martins NM, Anbu S, Mahmudov KT, Ravishankaran R, da Silva MF, Martins LM, Karande AA, Pombeiro AJ (2017) New J Chem 41:4076–4086
15. Ghanbari Z, Housaindokht MR, Izadyar M, Bozorgmehr MR, Eshtiagh-Hosseini H, Bahrami AR, Matin MM, Khoshkholgh MJ (2014) Sci World J 2014:1–10
16. Lange TS, Kim KK, Singh RK, Strongin RM, McCourt CK, Brard L (2008) PLoS ONE 3:e2303
17. Jana S, Chatterjee S, Chattopadhyay S (2012) Polyhedron 48:189–198
18. Connelly NG, Geiger WE (1996) Chem Rev 96:877–910
19. Sheldrick G (1998) SADABS v. 2.01, Bruker/Siemens area detector absorption correction program, Bruker AXS, Madison, Wisconsin, USA
20. Sheldrick GM (2015) Acta Crystallogr Sect A 71:3–8
21. Sheldrick GM (2015) Acta Crystallogr Sect C 71:3–8
22. Spek AL (2003) J Appl Crystallogr 36:7–13
23. Dolomanov OV, Bourhis LJ, Gildea RJ, Howard JA, Puschmann H (2009) J Appl Crystallogr 42:339–341
24. Dinsdale DR, Lough AJ, Lemaire MT (2015) Dalton Trans 44:11077–11082
25. Badetti E, Gjoka B, Nagy EM, Bernardinelli G, Kündig PE, Zonta C, Licini G (2015) Eur J Inorg Chem 2015:3478–3484
26. Palaniandavar M, Velusamy M, Mayilmurugan R (2006) J Chem Sci 118:601–610
27. Strautmann JBH, Freiherr von Richtofen C-G, Heinze-Bruckner G, DeBeer S, Bothe E, Bill E, Weyhermuller T, Stammler A, Bogge H, Glaser T (2011) Inorg Chem 50:155–171
28. Taylor RA, Bonanno NM, Mirza D, Lough AJ, Lemaire MT (2017) Polyhedron 131:34–39
29. Sirirak J, Harding DJ, Harding P, Liu L, Telfer SG (2015) Aust J Chem 68:766–773
30. Odhiambo RA, Muthakia GK, Kagwanja SM (2012) Transition Met Chem 37:431–437
31. Nivorozhkin AL, Anxolabéhère-Mallart E, Mialane P, Davydov R, Guilhem J, Cesario M, Audière J-P, Girerd J-J, Styring S, Schussler L (1997) Inorg Chem 36:846–853
32. Liu HK, Sadler PJ (2011) Acc Chem Res 44:349–359
33. Vančo J, Šindelář Z, Dvořák Z, Trávníček Z (2015) J Inorg Biochem 142:92–100
34. Biswas B, Mitra M, Pal A, Basu A, Rajalakshmi S, Mitra P, Aliaga-Alcalde N, Kumar GS, Nair BU, Ghosh R (2013) Indian J Chem 52A:1576–1583
35. Singh N, Pagariya D, Jain S, Naik S, Kishore N (2018) J Biomol Struct Dyn 36:2449–2462